Acta Cryst. (1988). A44, 449-461

Minimum Detectable Solute Concentration in Atomic-Resolution Transmission Electron Microscopy

BY J. M. HOWE, D. P. BASILE AND N. PRABHU

Department of Metallurgical Engineering and Materials Science, Carnegie Mellon University, Pittsburgh, PA 15213, USA

AND M. K. HATALIS*

Department of Electrical and Computer Engineering, Carnegie Mellon University, Pittsburgh, PA 15213, USA

(*Received 5 August 1987; accepted 2 February 1988*)

Abstract

The minimum solute concentration necessary to produce an observable change in image contrast in atomic-resolution transmission electron microscopy was investigated by multislice image-simulation techniques. The results show that local changes in specimen composition produce regular changes in image contrast, and that the minimum detectable solute concentration for any system of matrix and solute can be predicted from a simple formula based on a rule of mixtures, using only the atomic numbers of the matrix and solute elements. Optimum specimen and microscope conditions for observing local changes in specimen composition and the possibility of using atomic-resolution transmission electron microscopy for absolute determination of specimen composition are also discussed.

1. Introduction

The current 300–400 keV transmission electron microscopes with spherical aberration coefficients of about 1 mm possess point-to-point resolutions of 0·18–0·2 nm. Since this is sufficient to resolve the atomic structures of most metallic and ceramic materials in low-index zone axes, the acronym ARM (atomic-resolution microscopy) has become popular. Atomic-resolution capability is particularly important in the field of materials science, where it is often necessary to understand the atomic structure and composition of a material in order to explain its properties. While many researchers have investigated the possibilities and limitations of structural information that is available by ARM (Spence, O'Keefe & Iijima, 1978; Saxton & Smith, 1985; Self, Glaisher & Spargo, 1985), the compositional information that is contained in atomic-resolution images is just beginning to be systematically examined (Rose & Gronsky, 1986; Ourmazd, Rentschler & Taylor, 1986; Howe, Dahmen & Gronsky, 1987; Tanaka & Cowley, 1987). The ability to determine the solute concentration in individual columns of atoms has many important applications in materials science, such as allowing determination of the extent of solute segregation to dislocations, grain and interphase boundaries, permitting characterization of long-range order in small metastable strengthening precipitates, and determining the extent of interdiffusion and abruptness of interfaces in multilayered structures. This paper presents the results of an investigation aimed at determining the minimum concentration of solute that produces a significant change in the image contrast of a matrix of arbitrary atomic number. The results from this study yield a general relationship for predicting contrast effects in atomic-resolution images due to changes in specimen composition.

2. Background

In the multislice method for calculation of dynamical amplitudes and phases in ARM (Cowley & Moodie, 1957; Lynch & O'Keefe 1972; Goodman & Moodie, 1974; Self, O'Keefe, Buseck & Spargo, 1983), a specimen of thickness t is divided into N slices of thickness Δz along the electron-beam direction. The thickness Δz is often chosen as the unit-cell dimension parallel to the electron-beam direction for convenience. The crystal potential of each slice Δz is replaced by its two-dimensional projected potential $\varphi(x, y)$ and treated as a transmission function or phase grating. The amplitudes and phases of the electron wave function at the exit surface of a specimen of thickness $t = N\Delta z$ are found by successive propagation of an incident wave function through the transmission function of each slice, and through vacuum in between each slice.

2.1. *Effect of solute on image contrast*

Tanaka & Cowley (1987) recently investigated the dynamical diffraction effects of diffuse scattering due

* Now with Department of Computer Science and Electrical Engineering, Lehigh University, Bethlehem, PA 18015, USA.

0108-7673/88/040449-13$03.00

to point defects (solute) in crystals on the resulting images through theoretical formulations and multislice image simulations. Simulations of Au crystals including point defects without strain showed that the image contrast is localized in atomic size and relatively insensitive to the defect depth when the total crystal thickness is fixed. Tanaka & Cowley (1987) also compared the contrast from two point defects separated horizontally in the same and different slices and concluded that the images of paired defects appear separately and that the image features do not change drastically with the defect depth. Therefore, the wave field below a crystal can be treated independently at each atomic column, as in the column approximation (Howie & Basinski, 1969; Van Dyck, Van Tendeloo & Amelinckx, 1982). Furthermore, because the modulation of the fundamental reflection is small and each diffuse scattering event is very weak, the final wave field from a crystal may be a sum of waves due to each point defect in the first approximation and the contrast from a small number of defects in an atomic column can be simply related to the number of defects by a nonlinear expression.

2.2. *Minimum detectable solute concentration*

In the extreme cases an atomic column can be composed of either pure matrix or solute atoms. For a mixture of matrix and solute atoms, the average potential along the column will follow a rule of mixtures, as illustrated in Fig. 1. If it is assumed that the relative scattering power of any atom, and hence its projected potential, is adequately described by the atomic number Z, a rule of mixtures for scattering of electrons along a column of atoms may be written as

$$Z_A = Z_M(1-C) + CZ_S, \qquad (1)$$

where Z_M = atomic number of the matrix, Z_S = atomic number of the solute, Z_A = average atomic number of a column of atoms containing a concentration of solute C (atomic fraction or atomic percent). This investigation is particularly concerned with the minimum detectable solute concentration $C_{\min}$ that produces an observable effect in the image contrast since knowledge of $C_{\min}$ affords an estimate of the compositional sensitivity of ARM for any combination of matrix and solute. Equation (1) may therefore be arranged to give $C_{\min}$ as

$$C_{\min} = |Z_A - Z_M|/|Z_S - Z_M|, \qquad (2)$$

where the quantity $|Z_A - Z_M|$ represents the change in atomic number from the matrix required to produce an observable effect on the image contrast. Absolute values are used in (2) to ensure a positive value for $C_{\min}$. The logarithm of (2) yields

$$\log C_{\min} = -\log|Z_S - Z_M| + \log|Z_A - Z_M|. \qquad (3)$$

The form of (3) is similar to power-law expressions used for describing the dependence of contrast on atomic number based on mass thickness (Reimer, 1984), and is analogous to equations which are used in biological work and imaging of single atoms on substrates in scanning transmission electron microscopy (Isaacson, Langmore, Parker, Kopf & Utlaut, 1976; Reimer, 1984). The value of the quantity $|Z_A - Z_M|$ can be determined by plotting $\log C_{\min}$ *versus* $\log|Z_S - Z_M|$ for any matrix and solute and extrapolating a straight line with slope equal to -1 to $|Z_S - Z_M| = 1$. Once the intercept $|Z_A - Z_M|$ is determined, (2) may be used to predict the minimum detectable solute concentration for any system of matrix and solute.

It is evident from (2) that $C_{\min}$ increases with Z_M and decreases with increasing $|Z_S - Z_M|$ as expected from electron scattering theory. That is, for a matrix of arbitrary atomic number the minimum concentration of solute that is required to produce a significant change in image contrast increases as the atomic number of the matrix increases, and decreases as the atomic number difference between the matrix and solute increases. Such behavior is expected on the basis that more solute is necessary to produce a contrast change above a strong-scattering matrix than above a weak-scattering matrix and, similarly, that less solute is required to produce a contrast change when the atomic numbers of the solute and matrix are very different than when they are nearly the same.

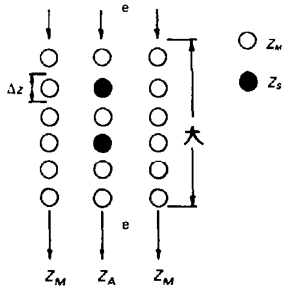

Fig. 1. Illustration of an average atomic number Z_A different from the matrix atomic number Z_M due to the addition of solute with atomic number Z_S.

2.3. *Optimum thickness for detection of point defects*

As illustrated in Fig. 2(*b*), a high-resolution image of a weak-phase object consists of dark atoms on a uniformly bright background (Spence, 1981), where the darkness increases with atomic number Z since the projected specimen potential is related to the atomic scattering amplitudes for electrons by an inverse Fourier transform (Hirsch, Howie, Nicholson, Pashley & Whelan, 1977). With increasing specimen thickness, dynamical diffraction causes the amplitudes of the Bragg-scattered beams to display an oscillatory (*Pendellösung*) dependence (Spence,

O'Keefe & Iijima, 1978). As illustrated in Fig. 2(*c*), when the specimen thickness reaches one-quarter of the extinction distance ($\xi_{000}/4$) and approaches one-half of the extinction distance ($\xi_{000}/2$), the intensity of the forward-scattered beam decreases and the image displays half-spacings arising from strong interference among the Bragg-scattered beams. For crystals between about $\xi_{000}/2$ and ξ_{000} thick, the dark spots lie among the atom positions, which leads to a reversal in image contrast (Figs. 2*d* and *e*), and at ξ_{000} the forward-scattered beam has its maximum intensity and the image shows somewhat reduced phase contrast (Fig. 2*f*). Since phase contrast is minimum at ξ_{000}, perturbations in the scattered amplitudes due to defects should show most strongly at this thickness (Self, Glaisher & Spargo, 1985; Rose, 1985). Based on this dynamical image behavior, it is expected that at Scherzer (1949) defocus, where the structural detail in an image is most easily interpreted, the maximum contrast due to defects such as impurities is most apparent at ξ_{000}, and this has been confirmed using high-resolution image simulations by Rose (1985), Rose & Gronsky (1986) and Tanaka & Cowley (1987). Since it is possible to produce specimens of most metallic and ceramic materials with thicknesses on the order of ξ_{000}, the possibilities of experimentally obtaining compositional information by ARM are favorable in this regard.

3. Experimental procedures

The experiments were performed by high-resolution image simulations, using the *SHRLI* suite of programs described by O'Keefe & Buseck (1979). The

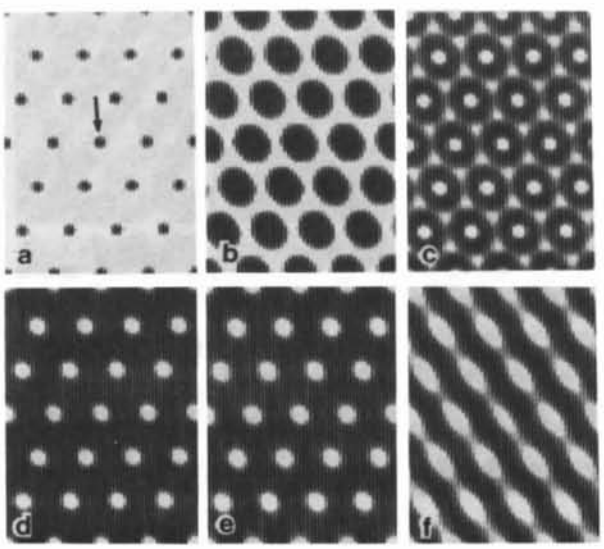

Fig. 2. (*a*) Projected potential for f.c.c. Al in a ⟨110⟩ orientation containing 2·5% Si in the center atomic column (arrow), and (*b*)–(*f*) simulated ARM images for the same structure at $\frac{1}{8}$, $\frac{1}{4}$, $\frac{1}{2}$, $\frac{3}{4}$ and ξ_{000}, respectively, where $\xi_{000} = 24{\cdot}4$ nm.

Table 1. *Elements (compounds), atomic numbers, crystal structures and orientations used to test equation* (2)

Element (compound)	Atomic number	Crystal structure	Zone axis
Al, Cu, Ag, Pt	13, 29, 47, 78	Face-centered cubic	⟨110⟩
Co	27	Hexagonal close packed	⟨11$\bar{2}$0⟩
Fe	26	Body-centered cubic	⟨100⟩
Si	14	Diamond cubic	⟨110⟩
GaAs, InP	31/33, 49/15	Zinc-blende	⟨110⟩

SHRLI suite consists of four programs, *FCO*128, *PG*128, *MS*128 and *IM*128, which are run in succession and use a 128 × 128 array to compute a simulated high-resolution electron microscope image. Images were calculated for a variety of compounds in order to determine the value of $|Z_A - Z_M|$ and test the range of validity of (2), using typical operating conditions for a perfectly aligned JEOL 4000EX microscope. The microsope operating conditions used in the simulations were: accelerating voltage (V) = 400 keV, spherical aberration coefficient (C_s) = 1·0 mm, objective lens defocus (Δf) = −50·0 nm, semi-angle of beam convergence (α) = 0·5 mrad, half-width of Gaussian spread-of-focus (Δ) = 5·0 nm and radius of objective aperture (r) = 6·0 nm^{-1}. The effects of nonaxial crystal and beam conditions are complicated and are not discussed in this analysis. The phase-grating slice thicknesses were taken as the interplanar spacing parallel to the electron-beam direction (for example, Δz in ⟨110⟩ Al was 0·286 nm), and at least those beams out to 40·0 nm^{-1} were included in the multislice calculations. The intensities from the simulated images were scaled so that each image contained intensities that ranged over the same grey levels. Although this normalization of image contrast means that low-contrast images have their intensity ranges stretched in comparison with images of inherently high contrast, most images had similar contrast and the majority of features were such that their intensity would be detectable on standard electron microscope photographic film. Similar manipulation of contrast can be performed using image processing techniques on digitized experimental images.

The compounds, crystal structures, atomic numbers and orientations examined in this study are presented in Table 1. The atomic numbers of the elements and compounds ranged from 13 to 78, and a variety of important crystal systems characteristic of structural metals, magnetic and semiconductor compounds were examined.

The general procedure used to determine the value of $|Z_A - Z_M|$ and test (2) was as follows. First, amplitude/phase *versus* thickness plots were generated for the pure elements and compounds. Subsequently, the concentration of solute was progressively increased in one column of the matrix and images were generated at exactly $\frac{1}{8}$, $\frac{1}{4}$, $\frac{1}{2}$, $\frac{3}{4}$ and ξ_{000}. It was found that

the maximum change in image contrast due to the solute occurred at ξ_{000} as expected from the discussion in § 2.3, and illustrated for 2·5% Si and Al in Fig. 2. This was true for the simple metallic structures as well as for the more complicated compound crystals and agrees with the findings of Rose & Gronsky (1986) for Si. The minimum detectable solute concentration C_{min} was then established by varying the solute concentration and performing further simulations at ξ_{000} until the change in image contrast was no longer readily apparent by eye. The eye was chosen to establish C_{min} because when an actual investigation is performed, an initial means of scanning an image for segregation *etc.* is likely to be done first by eye, followed by further digitization of the image and/or densitometer traces to obtain quantitative changes in the image intensity. Since there is no noise or surface contamination in the simulated images, there is essentially no limit to the detectability. However, Iijima (1977) has suggested that an intensity change of at least 3% is required for experimental detectability in actual images, and this was supported by the work of Rose (1985). In this investigation, C_{min} was selected to produce at least a 3% change in intensity and often about a 10% change. Since a value for C_{min} determined by eye is subjective, a representative example for C_{min} (2·5% Si in Al) is illustrated in Fig. 3(*c*).

After C_{min} was established for one solute, the value of the image intensity at the center of the solute-containing column I_S in Fig. 3(*e*) was determined from the *IM*128 program, and a percentage change in image intensity ($\%\Delta I$) relative to the center of a pure matrix column (I_M in Fig. 3*e*) was calculated from the formula $\%\Delta I = (I_S - I_M)(100)/I_M$. The intensity profile across the solute and matrix columns in Fig. 3(*e*) demonstrates that the intensity change due to the solute is confined within a single atomic column, and this agrees with the findings of Tanaka & Cowley (1987). An initial value of $|Z_A - Z_M|$ was also determined and a wide range of additional solutes with atomic numbers both greater and less than the matrix were individually added to the column. The value of C_{min} for each of these elements was established by achieving the same percentage change in image intensity ($\%\Delta I$) as the initial solute, which usually yielded the same change in image contrast, as demonstrated for various elements in Al in Fig. 4. In most cases, the percentage change in intensity at the solute column was between about 3 and 10%, usually being less when the atom positions were white than when they were dark, because it was easier to detect a change in image contrast with white atom positions. Furthermore, the effect of adding a

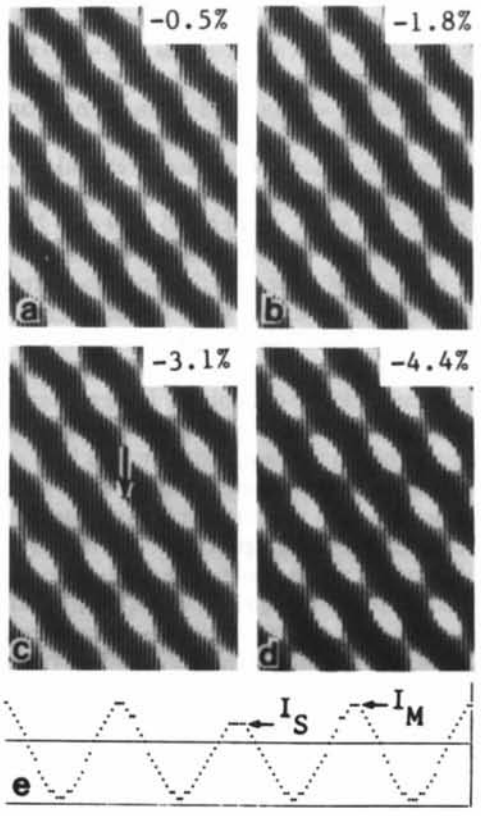

Fig. 3. (*a*)-(*d*) Simulated ARM images for f.c.c. Al in a ⟨110⟩ orientation and containing 0·5, 1·5, 2·5 and 3·5% Si in the center atomic column (arrow in *c*), and (*e*) intensity profile across the center row of atoms in (*c*), illustrating the decrease in intensity for the column containing Si (I_S) as compared with the intensity of a matrix column (I_M). The images are at ξ_{000} thickness and the percentage change in image intensity is shown in the top right-hand corner in (*a*)-(*d*).

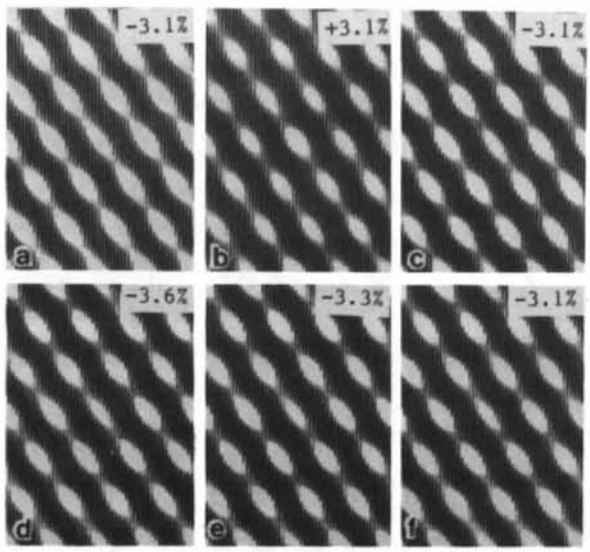

Fig. 4. Simulated ARM images for ⟨110⟩ Al containing: (*a*) 2·5% Si, (*b*) 2·0% Mg, (*c*) 0·4% Ca, (*d*) 0·3% Cu, (*e*) 0·15% Ag and (*f*) 0·09% Pt in the center atomic column. All images are at ξ_{000} and the solute concentrations are the values chosen for C_{min}. The corresponding intensity changes are shown in the top right-hand corners.

solute with an atomic number greater than the matrix was usually to cause the intensity to decrease at that position, *i.e.* more electron scattering (Figs. 4*a*, *c–f*), while adding a lighter solute caused the intensity to increase, *i.e.* less electron scattering (Fig. 4*b*). The values of C_{min} were then plotted *versus* $|Z_S - Z_M|$ on a log–log scale and a straight line with slope equal to -1 [equation (3)] was best fitted through the data points for each structure. The final value of $|Z_A - Z_M|$ was determined by taking the average of the values resulting from all of the structures, as discussed below.

4. Results and discussion

4.1. *Metallic elements*

The results for metallic structures are shown in Figs. 5 and 6. Two main features were examined for this group of elements: (1) the effect of changing atomic number on C_{min} for the same f.c.c. crystal structure, and (2) the effect of changing crystal structure (f.c.c., h.c.p., b.c.c.) on C_{min} for elements with similar atomic numbers. The results of the f.c.c. metals with atomic numbers ranging from 13 to 78 are shown in Fig. 5. In this figure, the experimental values of C_{min} were plotted and lines with slopes equal to -1 were best fitted through the data points. Although there is scatter in the data points about these lines, some of which is probably due to uncertainties in the values for the atomic scattering amplitudes, Fig. 5 shows that the expected behavior of increasing C_{min} with decreasing $|Z_S - Z_M|$ and increasing Z_M is realized, and that this behavior is reasonably well described by lines with slopes equal to -1, as predicted by (3). Furthermore, this behavior is displayed by all of the f.c.c. elements, independent of atomic number. Also note that in heavy matrices such as Pt, solutes with $|Z_S - Z_M| < 3$ are not detectable by eye, and that slightly better fits to the data would occur for all the elements if the slopes were decreased to about $-0{\cdot}8$ (dashed line for Al in Fig. 8), which indicates that (3) slightly underestimates the value of C_{min} when $|Z_S - Z_M|$ is greater than about 15 and slightly overestimates C_{min} when $|Z_S - Z_M|$ is less than this.

One unusual feature of the results in Fig. 5 is that the intercepts at $|Z_S - Z_M| = 1$ for Al and Cu are about six times less than those for Ag and Pt. That is, the intercepts for Ag and Pt (extrapolated above $C_{min} = 100\%$) are about $2Z_M$ while the intercepts for Al and Cu are about $\frac{1}{3}Z_M$. Examination of subsequent data in Figs. 6 and 8 shows that the values of $|Z_A - Z_M|$ for Al and Cu are exceptionally low, and that Ag and Pt display the most common behavior. The low intercepts for Al and Cu mean that addition of a small amount of solute produces a sharp change in image contrast for these elements, and this can be beneficial when looking for segregation *etc.*

The effect of changing crystal structure on C_{min} for nearly constant Z_M is illustrated in Fig. 6. Lines with slopes equal to -1 were best fitted through the data

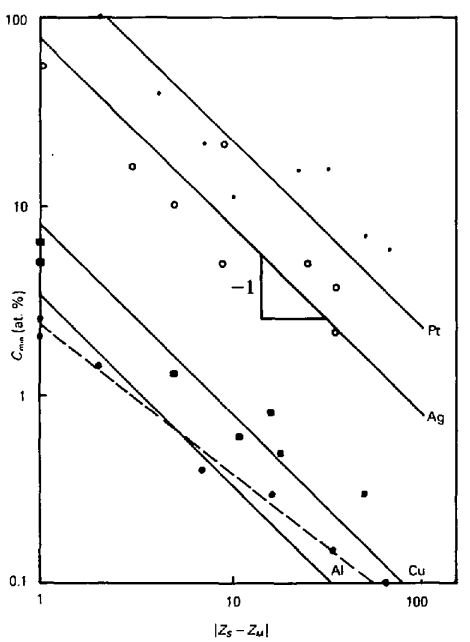

Fig. 5. Plot of log C_{min} *versus* log $|Z_S - Z_M|$ for ⟨110⟩ f.c.c. metals with atomic numbers of 13 (Al, $\xi_{000} = 24{\cdot}4$ nm), 29 (Cu, $\xi_{000} = 8{\cdot}2$ nm), 47 (Ag, $\xi_{000} = 5{\cdot}5$ nm) and 78 (Pt, $\xi_{000} = 18{\cdot}9$ nm). The dashed line corresponds to a slope of $-0{\cdot}8$ through the data for Al.

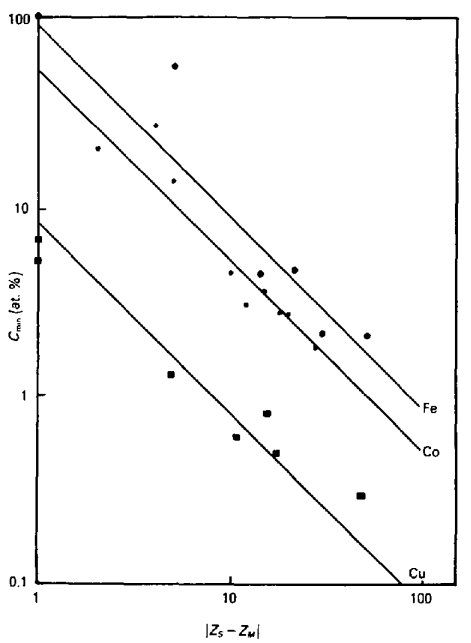

Fig. 6. Plot of log C_{min} *versus* log $|Z_S - Z_M|$ for metals with similar atomic numbers but different crystal structures and orientations, *i.e.* f.c.c. Cu (29, $\xi_{000} = 8{\cdot}2$ nm) in ⟨110⟩, h.c.p. Co (27, $\xi_{000} = 8{\cdot}5$ nm) in ⟨11$\bar{2}$0⟩ and b.c.c. Fe (26, $\xi_{000} = 16{\cdot}5$ nm) in ⟨100⟩.

for Fe (b.c.c.), Co (h.c.p.) and Cu (f.c.c.) with atomic numbers of 26, 27 and 29, respectively. Again, the dependence of C_{min} on $|Z_S - Z_M|$ is satisfactorily described by these lines although, as mentioned previously, the intercept for Cu (f.c.c.) is unusually low. The value of C_{min} at $|Z_S - Z_M| = 1$ for Co (h.c.p.) is about $2Z_M$ and consistent with Ag and Pt, while the intercept for Fe (b.c.c.) is significantly higher at about $3{\cdot}5Z_M$. These results indicate that crystal structure appears to affect C_{min} for constant Z_M. The way that crystal structure affects C_{min} can be explained by examining Fig. 7, where the minimum detectable concentrations of 4·3% Zr in Fe, 3·6% Mo in Co and 0·15% Ag in Cu (all with $|Z_S - Z_M| \sim 15$) are shown with the corresponding percentage changes in image intensity at the solute position. A 15% decrease in image intensity is required to observe contrast changes by eye in an open structure such as b.c.c. Fe, while only an 11% decrease is needed in the h.c.p. Co structure, and almost four times less intensity change (−3·3%) is required to cause observable effects in close-packed f.c.c. Cu as compared with h.c.p. Co. The reason for these changes appears to relate to the spacing, symmetry and intensity of the atom positions in these structures. When the atomic columns are widely separated, have a high projection symmetry and their images are dark on a bright background such as ⟨100⟩ Fe in Fig. 7(*a*), the addition of solute to a particular atomic column mainly affects the intensity only within the column without producing a large change in its shape or diameter. Since the atom positions are dark, a relatively large change in image intensity is required to be detectable by eye. In more closely packed structures with lower projection symmetry such as ⟨110⟩ Cu in Fig. 7(*c*), the addition of solute to a column produces a readily observable change in the image manifested as an increase or decrease in the size of the solute-atom position, particularly when the atomic columns are bright on a dark background. The h.c.p. ⟨11$\bar{2}$0⟩ Co is intermediate between these two cases.

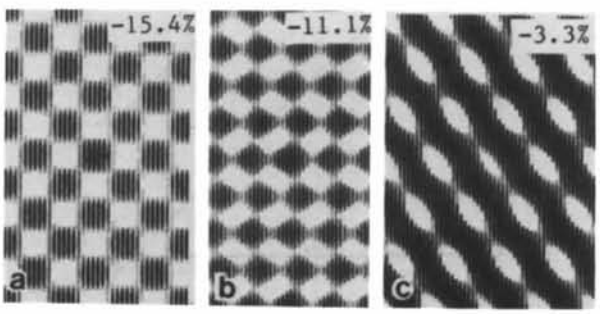

Fig. 7. Simulated ARM images at ξ_{000} for: (*a*) 4·3% Zr in Fe in a ⟨100⟩ orientation, (*b*) 3·6% Mo in Co in a ⟨11$\bar{2}$0⟩ orientation, and (*c*) 0·15% Ag in Cu in a ⟨110⟩ orientation. The corresponding intensity changes are shown in the top right-hand corners.

The previous observations yield an important result. If a common change in image intensity of $\Delta I = \pm 10\%$ is used to determine C_{min} rather than the eye, all of the data presented so far are accurately described by (3) and yield a common intercept of about $2Z_M$. Elements such as Al, Cu and Fe that have deviated from this behavior have done so because the eye has been used to determine the values of C_{min}. Therefore, (2) and (3) are essentially crystal-structure independent if the quantitative intensity change ($\%\Delta I$) is used to determine C_{min}, but appear to be crystal-structure dependent when the eye is used to determine C_{min}. Since (2) was derived using a rule of mixtures based only on the atomic numbers of the matrix and solute, it should be crystal-structure independent, and this behavior is confirmed if intensity changes only are used to determine C_{min}. This is discussed in greater detail in the next section.

4.2. *Diamond cubic and zinc-blende structures*

The results for diamond cubic (d.c.) Si and two zinc-blende compounds, GaAs and InP, are shown in Fig. 8. Three main features were examined with this second set of structures: (1) the dependence of C_{min} on $|Z_S - Z_M|$ in structures with a multiatom basis, (2) the effect of adding solute to either the lower (Z_L) or higher (Z_H) atomic-number position on C_{min} in a compound structure, and (3) the effect of having a small or large difference between Z_L and Z_H on C_{min} in compound structures. These features were examined to determine if a rule-of-mixtures approach

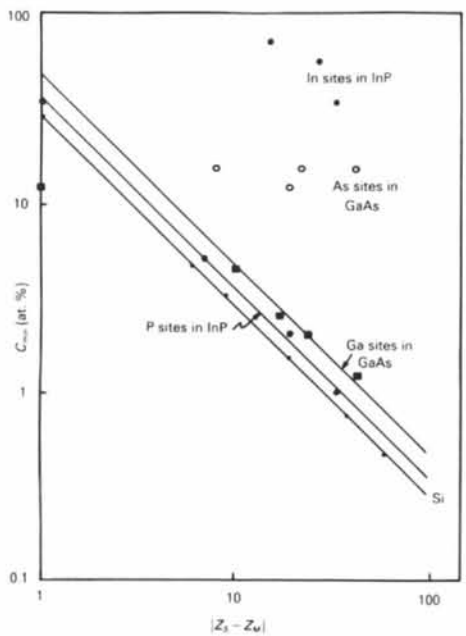

Fig. 8. Plot of log C_{min} *versus* log $|Z_S - Z_M|$ for ⟨110⟩ d.c. Si (ξ_{000} = 28·8 nm) and ⟨110⟩ GaAs (ξ_{000} = 14·4 nm) and InP (ξ_{000} = 33·2 nm) zinc-blende compounds.

Table 2. *Solute concentrations required to produce changes in the image intensity* ($\%\Delta I$) *on* As *sites in* GaAs

Solute	$\lvert Z_S - Z_L\rvert$	Predicted C_{min} for $2Z_M$	C_{min} by eye ($\%\Delta I$)	C_{min} at $\pm 10\%\Delta I$
Ge	1	64·0%	>100% (-)	24%
Nb	10	6·4%	15·0% (30·7)	4·5%
Si	17	3·8%	12·1% (73·1)	2·0%
Cs	24	2·7%	15·5% (36·3)	1·8%
W	43	1·5%	15·2% (15·9)	1·6%

is valid for predicting the effect of solute on image contrast in compound structures, or whether the image contrast is a more complex function which depends not only on the atomic number of the individual matrix column, but possibly also on the average atomic number of the compound, the atomic number difference between the compound atoms ($Z_H - Z_L$) or other factors. Each of these three effects is examined below.

The lines for Si, GaAs and InP in Fig. 8 were constructed by best fitting through the experimental data, as for the previous metallic structures. Examination of elemental Si (d.c.) shows that there is excellent agreement between experiment and theory, indicating that a rule of mixtures and (2) are valid for predicting C_{min} in structures with a multi-atom basis without additional complications. In addition, the value of the intercept at $\lvert Z_S - Z_M\rvert = 1$ is about $2Z_M$, which is consistent with the values obtained for elemental Co, Ag and Pt, and the C_{min} established by eye occurred for about a ±10% change in image intensity, so that this criterion also matched. Therefore, Si appears to be an ideal structure for testing (2) and determining the value of $\lvert Z_A - Z_M\rvert$, which is approximately $2Z_M$.

The data for solute on the Ga sites in GaAs also lie about a line with slope = −1 and an intercept of about $2Z_M$, except for $\lvert Z_S - Z_M\rvert < 10$, where they fall significantly below the line. In addition, the minimum detectable change in image contrast observed by eye occurred when the intensity change was about ±10%, so that C_{min} was similar regardless of which criterion was used. Thus, it appears that a rule of mixtures adequately describes the image behavior for adding solute to the Z_L positions in this compound, and that (2) can be used to determine C_{min} by substituting Z_L for Z_M. However, this behavior did not occur when solute was added to As sites in GaAs, and exceptionally high changes in image intensity (±30-75%) were usually required to produce observable effects in the image.

Therefore, using the eye to determine C_{min} resulted in values which were not described by $\lvert Z_A - Z_M\rvert \sim 2Z_M$, and the data did not fit to a line with slope = −1, as illustrated by the points included in Fig. 8, and shown in Table 2 for comparison with predicted values of C_{min} assuming $\lvert Z_A - Z_M\rvert = 2Z_M$. Also included in the last column of Table 2 are the C_{min} values which produced a ±10% change in image intensity. Although none of these concentrations produced an effect that was observable in the image by eye, the values for C_{min} generally agree within a factor of two with the predicted values of C_{min} for $\lvert Z_A - Z_M\rvert = 2Z_M$. This indicates that when the intensity rather than the eye is used to determine C_{min}, both (2) and a rule of mixtures are obeyed for the Ga and As sites in GaAs. For GaAs, it therefore appears that C_{min} can be determined with (2) by substituting either the value of Z_L or Z_H for Z_M, depending on which site the solute occupies, although it may not be possible to see the effect of the solute by eye. A further test of this is provided by the results from InP discussed below.

The effect of having a large difference in atomic number for the atoms in a compound structure was examined by adding solute to either the In or P sites in InP. This case should provide a good test of whether the addition of solute in a compound depends only on the atomic number of the column to which it is added, or if it is a more complex function of the average atomic number of the compound, *i.e.* $(Z_H + Z_L)/2$. As shown in Fig. 8, the data points for solute on the P sites in InP lie about a line with slope = −1 and an intercept of about $2Z_L$, indicating that C_{min} can be determined by using the atomic number of P (Z_L) for Z_M in (2). This confirms that the image intensity depends mainly on the atomic number of the column to which the solute is added (the column approximation) and that (2) is crystal-structure independent in compounds. It should be mentioned that the change in image intensity which was observable by eye was about ±10%, similar to solute on the Ga sites in GaAs, and that when solute was added to the In sites in InP, the same effect occurred as when solute was added to the As sites in GaAs. That is, exceptionally high values of C_{min} were required to produce an observable effect in the image by eye, and these values were not described by a line with slope = −1, as shown by the data in Fig. 8. However, when the values of C_{min} were determined for a ±10% change in image intensity, they also yielded a line with slope = −1 and an intercept of about $2Z_H$. Therefore, as for GaAs, (2) is valid for $\lvert Z_A - Z_M\rvert = 2Z_M$ when the percentage change in image intensity is used to determine C_{min} rather than the eye.

The reason for the apparent discrepancy between the C_{min} values determined by eye and by the percentage intensity change can be explained by examining the image contrast for the diamond cubic and zinc-blende structures in Fig. 9. The projected potential for InP is shown in Fig. 9(*a*) to illustrate the atomic positions in these structures with respect to the images. For elemental Si in Fig. 9(*b*), the atom pairs

in a ⟨110⟩ orientation appear as bright spots on a dark background. When solute is added to either of the atoms in the pair, the bright spot increases or decreases in size depending on whether Z_S is greater or less than that of Si, similar to many of the metallic structures discussed previously. This change in image contrast is readily detected by eye for an intensity change at the actual atom position of about ±10%. However, in both GaAs and InP, what appears to be asymmetric bright ovals or pairs consisting of bright and dim spots that might represent the different atoms in GaAs and InP are actually imaging effects, which are significantly displaced from the actual atom positions. In fact, in Figs. 9(*c*) and (*d*), the Z_L atoms lie in the narrow regions of the bright ovals and near the dim spots, while the Z_H atoms lie in the dark regions between the asymmetric bright ovals and bright spots, respectively. When solute is added to either the Ga or P sites, changes become apparent in the image for about a ±10% change in image intensity because the narrow regions of the bright ovals or the dim spots increase or decrease in size, similar to the behavior observed for solute in Si. However, when solute is added to the As or In sites, which reside in the dark regions of the image, an exceptionally high concentration of solute is required to produce an observable change in the image, although the intensity is changing consistently according to a rule of mixtures at lower concentrations.

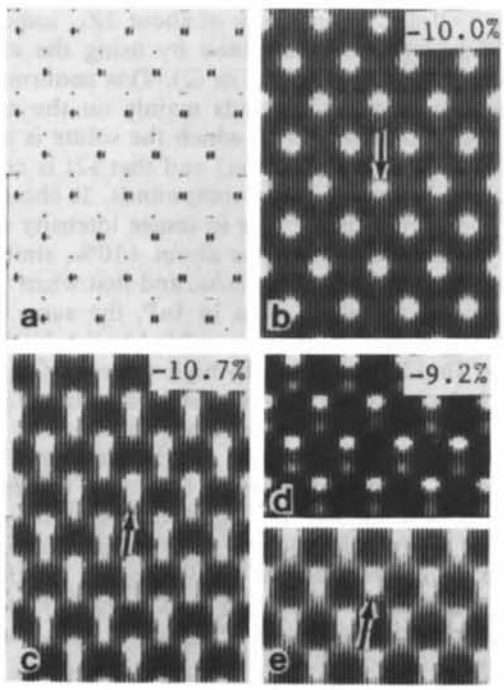

Fig. 9. (*a*) Projected potential for InP in a ⟨110⟩ orientation, (*b*) simulated ARM image for 3·0% As (arrow) in Si, with Si atoms in the same positions as the projected potential in (*a*), (*c*) simulated image for 4·5% Nb on the center Ga site (arrow) in GaAs, (*d*) simulated image for 10·0% Ti on the center P site (arrow in *e*) in InP, and (*e*) same as (*d*) except at −42·0 nm defocus. The percentage changes in image intensities are shown in the top right-hand corners.

Fig. 9(*e*) was included for comparison with Fig. 9(*d*) to illustrate that a small change in objective-lens defocus can be used to enhance the atomic number contrast in zinc-blende structures, as recently discussed by Ourmazd, Rentschler & Taylor (1986). Fig. 9(*e*) is identical to Fig. 9(*d*) except that the objective lens is at −42·0 nm defocus instead of Scherzer defocus (−50·0 nm). A defocus of −42·0 nm leads to asymmetric bright ovals in the image, similar to the image of GaAs in Fig. 9(*c*). Although the bright pairs are displaced from the actual atom positions as described for Fig. 9(*c*) above, the decrease in intensity at the solute position is more easily seen by eye in Fig. 9(*e*) than in Fig. 9(*d*), and this might be a preferred imaging situation when examining zinc-blende structures. The increase in image contrast that occurs between Z_H and Z_L elements in zinc-blende structures when the objective-lens defocus is decreased is due to diminution of the contrast transfer function at −42·0 nm defocus. This causes the structure-factor contrast carried in the 200 reflections to be enhanced at the expense of diminished structural information usually provided by the 220 reflections at −50·0 nm defocus (Ourmazd, Rentschler & Taylor, 1986). This effect increases with increasing $Z_H - Z_L$.

4.3. *Effects of specimen and microscope conditions*

Taking the average of the intercepts obtained for solutes in Ag, Pt, Co, Si, Ga sites in GaAs and P sites in InP yields a value of $|Z_A - Z_M| = 1{\cdot}8Z_M$. As mentioned in the analysis for the metallic elements, lines with a slope = −1 tend to slightly underestimate C_{min} when $|Z_S - Z_M|$ is larger than about 15, and to slightly overestimate C_{min} when this quantity is less. Therefore, replacing $|Z_A - Z_M|$ in (2) with $2Z_M$ compensates for the slight deviation from a slope of −1, and provides an accurate formula for estimating the minimum detectable solute concentration in any element or compound based purely on the atomic numbers of the solute and matrix column in which it resides. However, image contrast produced by adding solute to a matrix will vary with the microscope operating conditions, and there are other factors that might affect the image quality and hence the value of $|Z_A - Z_M|$ just determined. Some of these factors are considered in this section.

In all of the previous image calculations, the room-temperature Debye–Waller factors for the matrix and solute elements were kept constant at 0·4. This was done in order to isolate the effects of atomic number on image contrast. The effect of using the actual Debye–Waller factors for the elements may produce either lower or higher values of C_{min} than predicted

by (2) with $|Z_A - Z_M| = 2Z_M$, depending on the particular elements involved. In many cases, different Debye-Waller factors tend to increase the scattering difference between the matrix and solute and therefore decrease C_{min}. A second simplifying assumption used in order to isolate the effects of atomic number, that may not be satisfied in actual materials, was the absence of any strains in the lattice due to the difference in atomic volumes of the matrix and solute atoms. In many situations distortion of the matrix occurs during segregation, and this distortion may change the image contrast in the vicinity of the solute. However, as discussed by Dederichs (1973) and Tanaka & Cowley (1987), strains produce a different type of diffuse scattering than compositional changes, and the purpose of this investigation was to isolate and predict the effects of compositional changes only on the image intensity. A third assumption that was made was that the solute is random along the column. For very thin specimens, the image should be largely independent of the distribution of solute in the column. However, for specimens with thicknesses of ξ_{000}, the solute should have an increasingly strong effect on the image as it segregates towards the top surface because the diffuse scattering due to the solute has greater opportunity to interact dynamically with the Bragg-scattered beams. Rose (1985) investigated the effect of solute depth on the image contrast for an Sb impurity in an Si crystal ξ_{000} thick and found a gradual increase in contrast from the bottom (~8%) to $\xi_{000}/2$ (~20%) followed by a gradual decrease in contrast as the solute approached the top. Bursill & Shen (1984) found no contrast change with depth in the specimen in calculations on point defects in rutile and Tanaka & Cowley (1987) found little difference in the image contrast (intensity) due to point defects at different depths in Au, although the strongest contrast occurred when the fundamental reflections were strong, similar to Rose (1985). Since the solute in this investigation was averaged throughout the column, (2) should provide a reasonable estimate for C_{min} except when the solute is segregated to the bottom or center of the sample. In these situations, (2) may under- or overestimate the amount of solute required for detectability, respectively, although it still provides an indication of the contrast expected and an order-of-magnitude value for C_{min}.

The effects of noise and/or contamination on the specimen surface on the image were also neglected in this study, and these could be important considerations in compositional determination of actual specimens (Ponce & O'Keefe, 1986; Gibson, McDonald, Batstone & Phillips, 1987). However, high-resolution image simulation of defects in Si by Glaisher & Spargo (1983) indicate that noise may not limit interpretation. Furthermore, contamination did not appear to cause problems in recent compositional analyses of semiconductor compounds by Ourmazd, Rentschler & Taylor (1986) and Ourmazd (1987), which suggests that contamination may not pose severe limitations. Iijima (1977) has suggested that a contrast change of 3% is necessary for experimental detectability and this was satisfied for all of the C_{min} determined in this study. Since a ΔI of ±10% was found to agree best with the value of $|Z_A - Z_M| = 2Z_M$, it is concluded that the results described herein should be observable above background noise and contamination in many situations. It should also be emphasized that surface effects vary with the type of specimen and method of sample preparation, and this investigation considers the best possible case that can be obtained theoretically, with reasonable regard for practical application to real specimens. The effect of vacancies was not discussed in detail herein, but, to a first approximation, vacancies behave as if they have $Z_S \sim 1$ in (2). Furthermore, the specimen thickness has a major effect on the visibility of solute, as illustrated previously in Fig. 1. In this investigation, maximum visibility of solute was obtained at ξ_{000} for all of the crystal structures examined, in agreement with similar calculations of impurity segregation to dislocations in Si performed by Rose & Gronsky (1986). These results differ from those of Bursill, Shen, Smith & Blanchin (1984) and Bursill & Shen (1984), where the maximum visibility of small defects in nonstoichiometric rutile occurred at thicknesses of $(n+\frac{1}{2})\xi_{000}$. This difference may be due to the more complex crystal structure and defect models used in their investigation. Therefore, although (2) can be used to estimate C_{min} and predict changes in image contrast due to the addition of solute to a matrix, appropriate image calculations should be performed for very accurate interpretation in any particular system.

In addition to specimen conditions such as those mentioned above, certain variations in microscope parameters are known to change substantially the image contrast due to a defect. Some of the more important parameters are the objective aperture size (Reimer, 1984; Bursill, Shen, Smith & Blanchin, 1984; Rose & Gronsky, 1986) and position (Cowley, 1973), microscope accelerating voltage (Spence, 1981; Reimer, 1984), objective-lens defocus (Allpress & Sanders, 1973; O'Keefe, 1973; Cowley, 1975; Reimer, 1984; Ourmazd, Rentschler & Taylor, 1986) and crystal and beam alignment (Smith, Saxton, O'Keefe, Wood & Stobbs, 1983). While consideration of all these parameters is beyond the scope of this article, it is worth discussing the effects of several of these, in order to evaluate the possibility of using (2) with $|Z_A - Z_M| = 2Z_M$ for estimating C_{min} under slightly different microscope conditions and thereby extending the usefulness of the results.

As mentioned in the *Introduction*, the particular microscope parameters used in this investigation were for a perfectly aligned JEOL 4000EX at Scherzer

defocus. Scherzer defocus was chosen because it provides the optimum transfer of spatial information in most imaging situations. In addition, it has been shown (Reimer, 1984) that atomic-number contrast is maximum at Scherzer defocus. Since much of the effect of solute on image contrast is largely contained in diffuse scattering associated with the 000 beam, a reduction in phase contrast in the image enhances the amplitude contrast due to the solute. This effect is responsible for the maximum visibility of solute at ξ_{000}. A similar effect can be produced by decreasing the objective aperture size such that the fundamental specimen periodicities are eliminated from the image, as discussed by Cowley (1973), Reimer (1984), Rose & Gronsky (1986) and Bursill & Shen (1984). In this investigation, an objective aperture with $r = 6{\cdot}0\ \mathrm{nm}^{-1}$ was chosen because it represents an optimum size for many imaging situations; that is, it permits transfer of all the periodic information within the Scherzer resolution limit of the microscope but truncates high-order spatial frequencies which may reduce image contrast. The effect of increasing or decreasing the aperture size from $r = 6{\cdot}0\ \mathrm{nm}^{-1}$ on the contrast from a solute of concentration $C_{\min}$ is shown in Fig. 10. In this figure, it is apparent that increases in aperture size above $6{\cdot}0\ \mathrm{nm}^{-1}$ produce only minor effects on the image (Fig. 10*d*), as do decreases until about $4{\cdot}5\ \mathrm{nm}^{-1}$. Below about $4{\cdot}5\ \mathrm{nm}^{-1}$. the 111 fundamental reflections at $4{\cdot}3\ \mathrm{nm}^{-1}$ are excluded by the aperture resulting in a bright-field imaging situation, and the atomic number effect of the solute is dramatically enhanced at the expense of structural (phase) information (Figs. 1*a* and *b*). These results indicate that the value of $|Z_A - Z_M|$ will not vary greatly from $2Z_M$ for slight increases or decreases in aperture size ($\pm 1{\cdot}0\ \mathrm{nm}^{-1}$) about $r = 6{\cdot}0\ \mathrm{nm}^{-1}$.

Another practical consideration is the effect of accelerating voltage on the contrast due to solute. In general, contrast should increase with increasing accelerating voltage (Spence, 1981; Reimer, 1984). The effect of changing accelerating voltage with all other conditions constant is shown in Fig. 11. In these images, the solute (0·15% Ag in Al) produces a maximum change in the image intensity (−3·3%) at 400 keV, which is a positive indication about the capability of medium-voltage microscopes for observing compositional effects, although it should be noted that the images in Fig. 11 do not represent a one-to-one comparison, because the resolution of the microscope increases as the accelerating voltage increases in these images, as does the size of the objective aperture relative to the diffraction pattern. Nevertheless, the percentage intensity changes as a function of accelerating voltage from 200–800 keV indicate that the contrast variations are similar enough that (2) with $|Z_A - Z_M| = 2Z_M$ can be used to obtain readily estimates of $C_{\min}$ for most of the 300–400 keV microscopes currently available.

Other critical parameters in determining contrast from compositional changes are crystal and beam tilt.

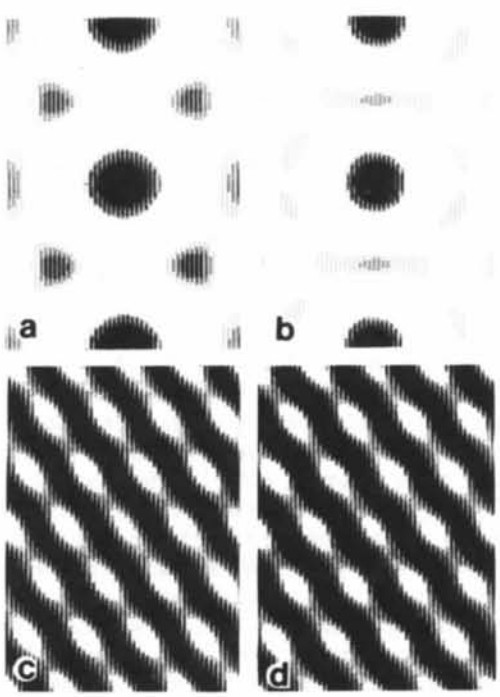

Fig. 10. Image contrast for 2·5% Si in Al with objective apertures of: (*a*) $r = 3{\cdot}0$, (*b*) $r = 4{\cdot}0$, (*c*) $r = 6{\cdot}0$ and (*d*) $r = 8{\cdot}0\ \mathrm{nm}^{-1}$. The solute is in the center atomic column, and additional contrast apparent at the top and bottom of (*a*) and (*b*) is due to the unit cells used in the image calculation.

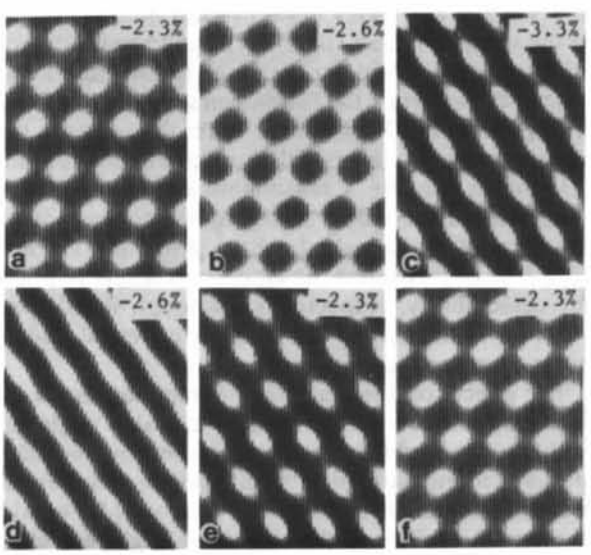

Fig. 11. Image contrast for 0·15% Ag in ⟨110⟩ Al at accelerating voltages of: (*a*) 200 ($\xi_{000} = 23{\cdot}0$ nm), (*b*) 300 ($\xi_{000} = 23{\cdot}8$ nm), (*c*) 400 ($\xi_{000} = 24{\cdot}3$ nm), (*d*) 500 ($\xi_{000} = 23{\cdot}8$ nm), (*e*) 600 ($\xi_{000} = 23{\cdot}4$ nm) and (*f*) 700 keV ($\xi_{000} = 23{\cdot}2$ nm). The corresponding intensity changes at the solute position are also shown.

In the present investigation, it was assumed that the microscope and specimen were perfectly aligned because this represents an optimum situation for observing a simple correspondence between image contrast and solute concentration. Examination of the effects of crystal and beam tilt shows that they detract from the simple relationship described above. The amounts of crystal and beam tilt that are required to produce a substantial change in image contrast are less for compound structures than for simple metals (Smith, Saxton, O'Keefe, Wood & Stobbs, 1983) and may be as little as a milliradian, depending on the system. These relationships are complicated and will be discussed in a subsequent paper.

4.4. *Limits of applicability*

Many different types of compositional variations can be found in materials. Random segregation of solute to regions of tension or compression along a dislocation represents somewhat linear segregation to which the present study may be applicable, and this has been investigated for Si by Rose & Gronsky (1986). Interdiffusion of elements across semiconductor interfaces and in multilayer materials are other examples where compositional variations may extend only a few atomic planes into an adjacent material (Ourmazd, 1987), and the effects of such compositional changes on image contrast may be approximately described using the treatment herein. This type of problem is common in materials science. The analysis of short-range order as described by Tanaka & Cowley (1987) is another example where this information is useful for interpreting image contrast. These are examples of spatially small compositional variations which are expected to produce relatively small changes in the amplitudes and phases of the fundamental reflections. The results may also be applicable to local clustering of solute into volume defects such as GP zones. However, when large composition changes occur over large spatial regions, for example in spinodal decomposition and growth of highly ordered precipitates, interpretation of image contrast is much more complicated. While the simple results that increasing the atomic number in a column of atoms darkens the column and decreasing the atomic number lightens the column can still be useful for deducing compositional changes in these situations (Howe, Dahmen & Gronsky, 1987), the contrast effects described in this paper can only serve as a guide to possible image contrast rather than as a predictor of contrast.

4.5. *Image contrast from* 0 *to* 100% *solute*

The previous sections have concentrated on determining C_{min} and the validity of (2). Another related question that was examined in this investigation is the possibility of using ARM for absolute determination of specimen composition. This has many

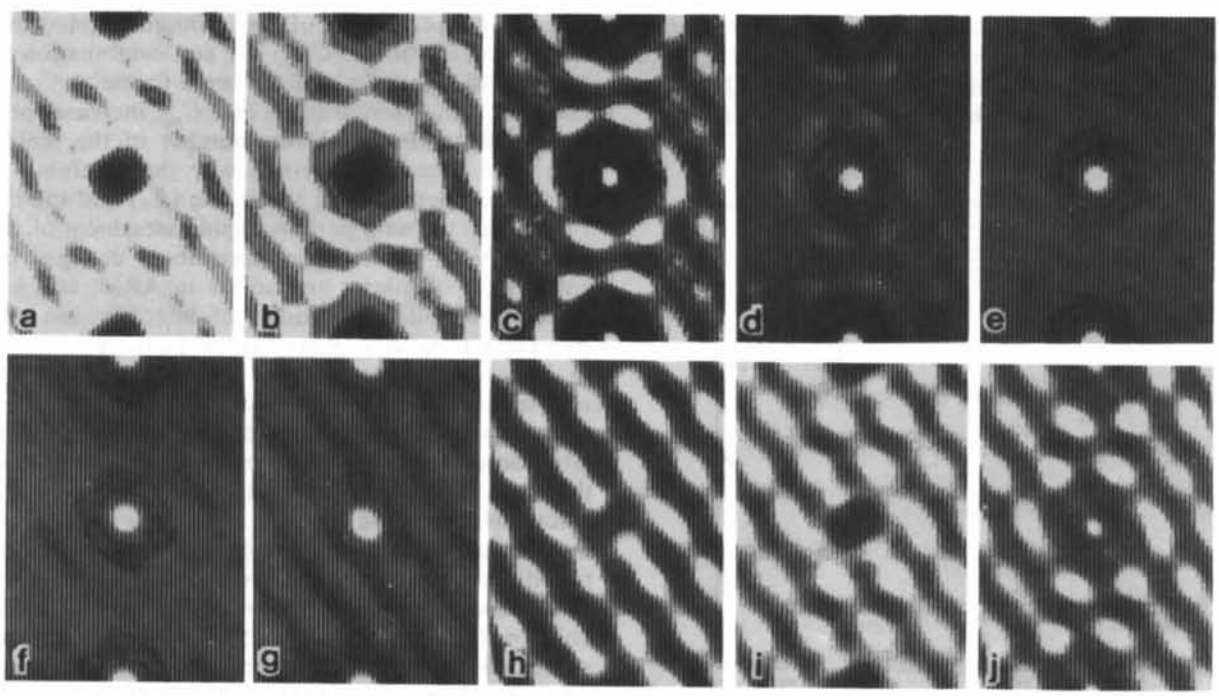

Fig. 12. (*a*)-(*j*) Simulated ARM images for ⟨110⟩ Al containing 10 to 100 at.% Cu in concentration intervals of 10 at.%. The solute is in the center of the image, and additional contrast at the top and bottom is due to the unit cells used in the calculations. The crystal thickness is $\xi_{000} = 24{\cdot}4$ nm.

important applications in materials analysis, such as for determining the compositions of GP zones, interdiffusion at interfaces *etc.* Results from Cu in Al are shown in Figs. 12(*a*)-(*j*), at concentration intervals of 10 at.% solute. As the solute content is increased above C_{min} (refer to Fig. 4*d*), major changes in both the image appearance and intensity at the solute position occur. Furthermore, both the image intensity and appearance vary asymmetrically about 50% solute as shown in Fig. 13 and as seen by comparing Figs. 12(*c*) and (*g*) or 12(*b*) and (*h*). Thus, while it may be difficult to determine the absolute composition to within ±15% for compositions in the range of 40-60% Cu from either the image contrast or percentage intensity change alone, using both data allows the solute composition to be determined to within a few percent. Therefore, the possibility of absolute composition determination by ARM appears promising when both images and intensities are used, and future advances in image processing may facilitate this situation.

Another important point evident from the data in Fig. 13 is that the intensity change is not a linear function of solute concentration, as discussed by Tanaka & Cowley (1987). Therefore, while the rule of mixtures and the development in § 2.2 are valid for describing the dependence of the minimum detectable solute concentration on atomic number and for relating the intensity of an atomic column with the solute content for small intensity changes, more complicated expressions are required to describe the dependence of image contrast on solute concentration for any combination of matrix and solute. Effects similar to those shown in Fig. 13 were found for other elements and compounds examined in this study.

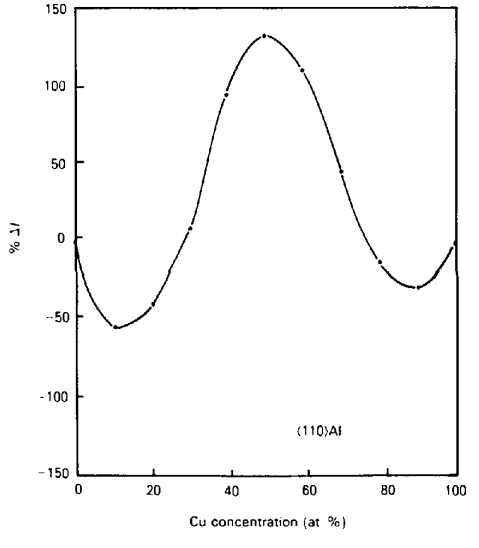

Fig. 13. Percentage change in image intensity as a function of atomic percent Cu in ⟨110⟩ Al.

Concluding remarks

The results of this investigation demonstrate that local variations in specimen composition produce regular changes in the image contrast in ARM, and that it is possible to describe these effects quantitatively by considering only the atomic numbers of the matrix and solute atoms. Since the image contrast in ARM depends on both specimen and microscope conditions, optimum values of these parameters for observing changes in specimen composition while retaining atomic structural information are defined. The optimum specimen thickness and microscope defocus for simultaneous observation of intensity changes in the image due to composition and structural variations in most imaging situations are ξ_{000} and Scherzer defocus, respectively. The optimum objective aperture size for observing the atomic structure of a specimen by phase contrast at 300-400 keV with enhanced composition effects through amplitude contrast appears to be one that circumscribes the fundamental specimen periodicities and eliminates spatial frequencies beyond the Scherzer resolution limit. Given the above operating conditions, the contrast changes arising from addition of solute to a matrix can be accurately described by a rule-of-mixtures approach based solely on the atomic numbers of the matrix and solute. This treatment shows that the average atomic number of a column containing solute must increase or decrease by a factor of about twice the atomic number of the matrix before the solute becomes visible. It also allows prediction of the minimum detectable solute concentration (C_{min}) for any combination of matrix and solute through a simple formula, $C_{min} = 2Z_M/|Z_S - Z_M|$, which states that C_{min} increases proportionally with the atomic number of the matrix (Z_M) and decreases inversely with the difference in atomic number between the solute (Z_S) and matrix. Use of this formula permits rapid assessment of the possibility of observing compositional changes for any system of matrix and solute in ARM, and has wide applicability to studies of interdiffusion and interfacial roughness in multilayered structures, order in metastable strengthening precipitates *etc.* The results also demonstrate that for low solute concentrations with the microscope conditions described above, addition of a solute with lower atomic number than the matrix causes an increase in the intensity at the solute column while addition of a solute with higher atomic number causes a decrease in intensity. Additionally, the results show that with ARM it is possible to determine the composition of individual atomic columns to within at least ±15% in many cases, and sometimes to within a few percent if both image and intensity data are available. The rule-of-mixtures approach to contrast prediction in ARM is essentially crystal-structure independent when intensity measurements are used to judge changes in image

contrast but is crystal-structure dependent when the eye is used to determine changes in image contrast. Thus, quantification of image intensities should be used for accurate composition determination by ARM. Lastly, although this study only considers systems containing two elements, the results indicate that similar principles can be used to interpret the contrast in systems containing combinations of three or more elements.

The authors are grateful to Dr M. A. O'Keefe for a critical review of this manuscript and to Dr J. Rose for several helpful discussions. This research was partially supported (JMH) by the National Science Foundation under Contract No. DMR-8657215. The authors also acknowledge N. Monda and Carnegie Mellon University for providing the computer funding.

References

ALLPRESS, J. G. & SANDERS, J. V. (1973). *J. Appl. Phys.* **6**, 165–190.
BURSILL, L. A. & SHEN, G. J. (1984). *Optik (Stuttgart)*, **66**, 251–276.
BURSILL, L. A., SHEN, G. J., SMITH, D. J. & BLANCHIN, M. G. (1984). *Ultramicroscopy*, **13**, 191–204.
COWLEY, J. M. (1973). *Acta Cryst.* A**29**, 529–540.
COWLEY, J. M. (1975). *Diffraction Physics*, pp. 283–292. Amsterdam: North-Holland.
COWLEY, J. M. & MOODIE, A. F. (1957). *Acta Cryst.* **10**, 609–619.
COWLEY, J. M. & MOODIE, A. F. (1958). *Proc. Phys. Soc.* **70**, 533–552.
DEDERICHS, P. H. (1973). *J. Phys. F*, **3**, 471–496.
GIBSON, J. M., MCDONALD, M. L., BATSTONE, J. L. & PHILLIPS, J. M. (1987). *Ultramicroscopy*, **22**, 35–46.
GLAISHER, R. W. & SPARGO, A. E. C. (1983). *Inst. Phys. Conf. Ser.* No. 68, pp. 185–190.
GOODMAN, P. & MOODIE, A. F. (1974). *Acta Cryst.* A**30**, 280–290.
HIRSCH, P., HOWIE, A., NICHOLSON, R. B., PASHLEY, D. W. & WHELAN, J. (1977). *Electron Microscopy of Thin Crystals*, pp. 201–207. Malabar: R. E. Krieger.
HOWE, J. M., DAHMEN, U. & GRONSKY, R. (1987). *Philos. Mag.* A**56**, 31–61.
HOWIE, A. & BASINSKI, Z. S. (1969). *Philos. Mag.* **149**, 1039–1063.
IIJIMA, S. (1977). *Optik (Stuttgart)*, **48**, 193–208.
ISAACSON, M. S., LANGMORE, J., PARKER, N. W., KOPF, D. & UTLAUT, M. (1976). *Ultramicroscopy*, **1**, 359–376.
LYNCH, D. F. & O'KEEFE, M. A. (1972). *Acta Cryst.* A**28**, 536–548.
MOTT, N. F. (1930). *Proc. R. Soc. London Ser. A*, **127**, 658–672.
O'KEEFE, M. A. (1973). *Acta Cryst.* A**29**, 389–401.
O'KEEFE, M. A. & BUSECK, P. R. (1979). *Trans. Am. Crystallogr. Assoc.* **15**, 27–46.
OURMAZD, A. (1987). *Proc. 45th Annual Meeting EMSA*, pp. 332–333. San Francisco: San Francisco Press.
OURMAZD, A., RENTSCHLER, J. R. & TAYLOR, D. W. (1986). *Phys. Rev. Lett.* **57**, 3073–3076.
PONCE, F. A. & O'KEEFE, M. A. (1986). *Proc. 44th Annual Meeting EMSA*, pp. 522–525. San Francisco: San Francisco Press.
REIMER, L. (1984). *Transmission Electron Microscopy, Principles of Image Formation and Microanalysis*, pp. 185–222. Berlin: Springer-Verlag.
ROSE, J. (1985). PhD Thesis. Univ. of California, Berkeley, USA.
ROSE, J. & GRONSKY, R. (1986). *Materials Problem Solving with the Transmission Electron Microscope*, pp. 57–64. Pittsburgh: MRS.
SAXTON, W. O. & SMITH, D. J. (1985). *Ultramicroscopy*, **18**, 39–48.
SCHERZER, O. (1949). *J. Appl. Phys.* **20**, 20–29.
SELF, P. G., GLAISHER, R. W. & SPARGO, A. E. C. (1985). *Ultramicroscopy*, **18**, 49–62.
SELF, P. G., O'KEEFE, M. A., BUSECK, P. R. & SPARGO, A. E. C. (1983). *Ultramicroscopy*, **11**, 35–52.
SMITH, D. J., SAXTON, W. O., O'KEEFE, M. A., WOOD, G. J. & STOBBS, W. M. (1983). *Ultramicroscopy*, **11**, 263–282.
SPENCE, J. C. H. (1981). *Experimental High-Resolution Electron Microscopy*, pp. 72–88. Oxford: Clarendon.
SPENCE, J. C. H., O'KEEFE, M. A. & IIJIMA, S. (1978). *Philos. Mag.* A**38**, 463–482.
TANAKA, N. & COWLEY, J. M. (1987). *Acta Cryst.* A**43**, 337–346.
VAN DYCK, D., VAN TENDELOO, G. & AMELINCKX, S. (1982). *Ultramicroscopy*, **10**, 263–280.

Acta Cryst. (1988). A**44**, 461–467

On the Treatment of Primary Extinction in Diffraction Theories Based on Intensity Coupling

BY JOCHEN R. SCHNEIDER, ODAIR D. GONÇALVES* AND HANS A. GRAF

Hahn-Meitner-Institut, Glienicker Strasse 100, *D*-1000 *Berlin* 39, *Federal Republic of Germany*

(*Received* 12 *June* 1987; *accepted* 11 *February* 1988)

Dedicated to Ulrich Bonse on the occasion of his 60th birthday

Abstract

Czochralski-grown silicon crystals of approximately 10 cm diameter and 1 cm thickness have been annealed at 1470 K in order to create a homogeneous defect structure, which is a basic condition for all statistical treatments of extinction. Absolute values of the integrated reflecting power of the 220, 440 and 660 reflections have been measured with 0·0392 Å γ-radiation in symmetrical Laue geometry for sample thicknesses between 1 and 3 cm. The amount of extinction in the experimental data varies between $y \simeq 0{\cdot}95$ and $y \simeq 0{\cdot}05$. Darwin's extinction theory has been used to describe the thickness dependence of the data sets. Despite some shortcomings of the model, it is shown that the assumption of a physically

* On leave from Instituto de Fisica, Universidade Federal do Rio de Janeiro, 21910 Rio de Janeiro RJ, Brazil.

0108-7673/88/040461-07$03.00